COMPARISON OF HIMAWARI-8 SATELLITE RADIANCE DATA ASSIMILATION METHODS FOR EXTREME RAINFALL PREDICTION IN EAST KALIMANTAN, JUNE 2nd – 4th, 2019

Huda Abshor Mukhsinin[1,2]*, Nurjanna Joko Trilaksono[1]
[1] Faculty of Earth Sciences and Technology, Bandung Institute of Technology, Jl. Ganesha 10, Bandung, Indonesia
[2]Indonesia Meteorological Climatological and Geophysics Agency, Jl. Angkasa I 2 Kemayoran, Central Jakarta, Indonesia
*****_E-mail: huda.mukhsinin@bmkg.go.id_

Received: August 19, 2024 Reviewed: November 25, 2024 Accepted: July 15, 2025

ABSTRACT

The performance of assimilating Himawari-8 satellite radiance data on a convection-permitting model (CPM) depends on the methods of assimilation. Hence, in this study, we compared the impact of different assimilation methods of Himawari-8 satellite radiance data on a CPM's prediction skills for the case of extreme rainfall in East Kalimantan, June 2nd – 4th, 2019. The study tested four schemes on the Weather Research and Forecasting (WRF) model at 3 km resolution, comparing a scheme without assimilation (NODA) and three schemes with different assimilation methods: 3DVAR, and Hybrid 3DEnVar (HYBRID, and DUALRES). Results showed that assimilation with hybrid 3DEnVar and 3DVAR techniques significantly improved the prediction skill of extreme rain, for instance, a 25% improvement of the true positive rate. The DUALRES scheme excelled in reducing biases in rainfall distribution. It was found that assimilation with the 3DEnVar method, particularly the DUALRES scheme, improved the prediction sensitivity to complex atmospheric dynamics, produced more accurate rainfall distribution and intensity, and improved the diurnal pattern of rainfall in East Kalimantan.

Keywords: Himawari-8, 3DVAR, Hybrid 3DEnVar, East Kalimantan, WRF

1. Introduction

East Kalimantan, located on one of the largest islands in the Indonesian Maritime Continent (IMC), experiences a unique weather pattern characterized by deep convection in the mid night caused by a diurnal cycle of land-sea breezes [1] as well as the extreme rainfall case that occurred in East Kalimantan on June 2nd – 4th, 2019 caused extensive damage to the region, resulting in flooding and landslides. However, to resolve the deep convection motion of this area, a model with the ability to describe the non-hydrostatic dynamic and fine horizontal (and vertical) grid resolution even smaller than the updraft scale of deep convection is essential [2]. The use of convection-permitting models (CPMs) is crucial for accurate rainfall prediction, especially when simulating rain patterns in the IMC, which is characterized by strong diurnal circulation [1,3]. However, effectively predicting rainfall using this model remains a challenge due to convection instability and significant variations in limited spatial and temporal scales. The rapid changes of convection in IMC need the initial condition that represents its background flow [4-6], thus assimilation is implemented to improve the initial condition to produce a more accurate simulation.

Utilizing the radiance data obtained from geostationary satellites is crucial for improving the initial condition in CPMs. Geostationary satellites orbit the Earth at a fixed position, approximately 35,786 km above the Earth's surface, allowing them to provide high-resolution observations over extensive areas. This capability enables continuous monitoring of atmospheric conditions [7]. On October 7, 2014, the Japan Meteorological Agency (JMA) successfully launched one of its Geostationary Meteorological Satellites (GMS), the Himawari-8. The satellite orbits at an altitude of 35,800 km above the equator at a nadir of 140.7° E, covering an observation area of 80° E to 160° W and 60° N to 60° S. The Himawari-8 satellite has the latest generation of infrared and visible sensors called the Advanced Himawari Imager (AHI). AHI observes the Earth's atmosphere with more visible, near-infrared, water vapor infrared, and surface-sensitive infrared channels than its predecessor, the Multi-functional Transport Satellite (MTSAT) or Himawari-7 [8]. The AHI sensor features 16 observation channels, with 10 of them being infrared (IR) channels crucial for numerical weather prediction. Notably, channels 8, 9, and 10 (at 6.25, 6.95, and 7.35 μm) are adept at detecting water vapor in the atmosphere [9] and have been utilized as valuable assimilation data [10,11].

AHI has played a critical role in the development of numerical weather prediction (NWP) systems by providing essential assimilation data. On a global scale, the assimilation of radiance AHI has significantly improved short- and mid-range water vapor prediction parameters [12]. On a regional scale, the assimilation of radiance AHI simulated wetter atmospheric conditions for the low-to-mid troposphere [8]. The assimilation of radiance AHI data also showed significant improvement in the tropical cyclone case study indicating that the assimilation of AHI data can improve the analysis of tropical cyclone structure and intensification, decrease the error value in tropical cyclone prediction, and improve the analysis of convection initialization and distribution significantly [13-16]. In addition, AHI data assimilation at the convective scale was carried out several times in the mid-latitude region, which showed an improvement in the analysis of prediction models in simulating atmospheric conditions and an increase in rainfall prediction skills [11,17-21]. Despite the assimilation of radiance AHI improved the rainfall prediction skills, the effectivity of prediction skills depends on the assimilation methods.

The three dimensional variational (3DVar) assimilation technique has been successful and widely used due to its computational efficiency. However, this method does not consider the actual flow-dependency of the system. This is due to the assumption that the background error covariance is homogeneous, isotropic, and does not change over time. On the other hand, the Ensemble Kalman Filter (EnKF) method is a better alternative in variant data assimilation systems because it takes into account the flow-dependency of its ensemble and is easy to implement [22]. However, in smaller ensembles (~20 to 100 members), EnKF has the disadvantage of ranking and thus the background error covariance can be affected by sampling errors which can result in spurious correlations at distantly separated locations [23]. To address these issues, hybrid ensemble-variational (EnVar) methods for instance 3D-Ensemble-Variational (3DenVar) offer methods that utilize the strengths of both variational and EnKF methods, thereby overcoming the ranking shortcomings caused by ensemble size constraints, as well as the static, homogeneous, and isotropic covariances caused by 3DVAR assumptions [24]. Therefore, in this study, we compare the assimilation of Himawari-8 satellite radiance data between 3DVar and 3DEnVar assimilation techniques to investigate how much the assimilation methods differ in improving the prediction skill of extreme rain in East Kalimantan on a convective scale.

2. Methods

This research is an experimental study that utilizes the Weather Research and Forecasting (WRF) limited area model version 4.5 with the Advanced Research WRF (WRF-ARW) dynamical core alongside the WRF *Data Assimilation* (WRFDA) module [25]. Initial conditions and boundary conditions generated from the National Centers for Environmental Prediction-Global Forecast System (NCEP-GFS) model followed by dynamical downscaling using the two-way nesting method with two domains as shown in Figure 1. The parent domain grid (d01) is 9 km with total grid points of 285 × 285 while the inner domain grid (d02) is 3 km with grid points of 268 × 268. The domain is set to 41 vertical layers with a peak at 50 hPa and a time step every 30 seconds. The physical parameterizations used in d01 and d02 include the following: WRF Single-Moment-6-class microphysical scheme [26], planetary boundary layer scheme Yonsei University [27], longwave radiation Rapid Radiative Transfer Model [28], shortwave radiation Dudhia scheme [29], Noah land surface model [30], and Kain-Fritsch cumulus parameterization [31] which is only enabled in d01.

A total of 4 experimental schemes were designed. The first scheme is a WRF model without assimilation (NODA). This model uses initial and boundary condition data interpolated directly from the NCEP-GFS model. The second scheme is a WRF model assimilated using the 3DVAR method (3DVAR). The third scheme is the WRF model assimilated using the hybrid 3DEnVar (HYBRID) method. In the 3DVAR method, the static background error covariance is generated through the NMC (National Meteorology Centre) method [32] which calculates the average difference between the 24-hour and 12-hour predictions at the validation time for one month in the previous year. On the other hand, in the 3DEnVar hybrid method, the background error covariance is a combination of static and flow-dependent covariance. Although the HYBRID method has the advantage of utilising flow-dependent covariance information, it still requires expensive computation to produce a model with full ensemble resolution. Therefore, to reduce the computational cost resulting from the HYBRID scheme, this study also applies a fourth assimilation scheme, namely the 3DenVar assimilation scheme with the dual resolution (DUALRES) method. The DUALRES scheme is a scheme that utilises flow-dependent information from the low-resolution ensemble into the high-resolution ensemble to be analysed as the background error covariance [33].

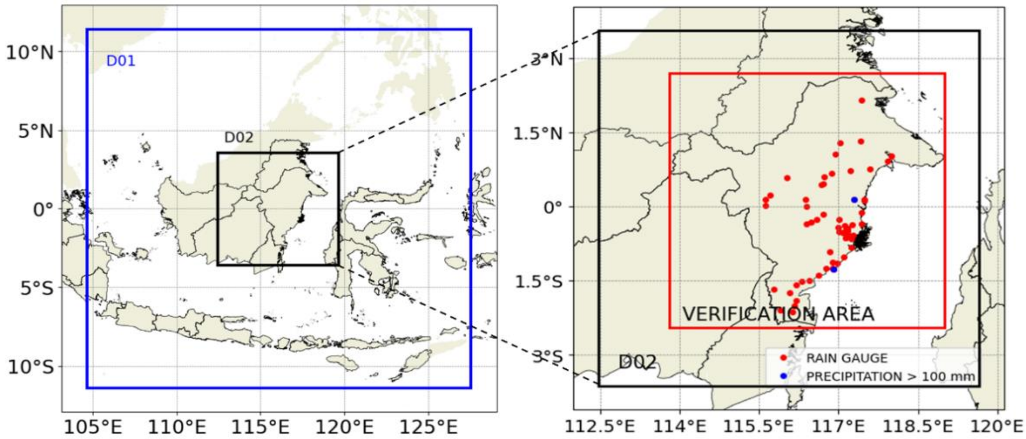

Figure 1. Experimental domain configuration of the WRF model. The red frame is the spatial verification area for East Kalimantan, the red dots show the location of the rain gauges, and the blue dots show the accumulated 24-hour rainfall above 100 mm.

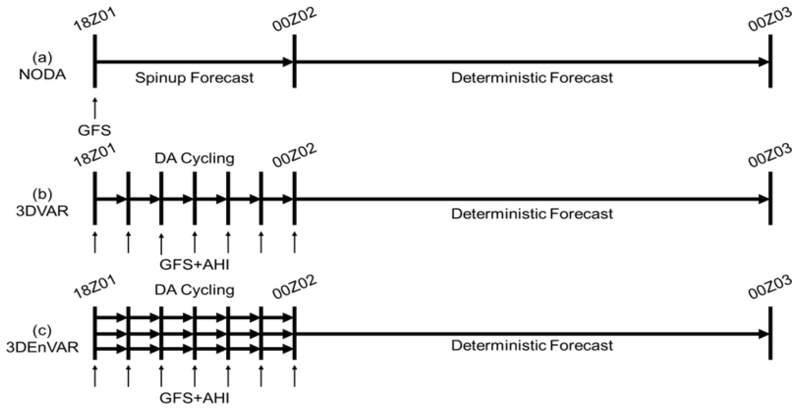

Figure 2. WRF model experiment flow (a) without assimilation, (b) with 3DVAR AHI assimilation, and (c) with 3DEnVar AHI assimilation (3 parallel lines illustrate the initial conditions on ensemble members which are then taken as the ensemble mean to produce deterministic predictions for the next 24 hours.

The experimental procedure is illustrated in Figure 2. The NODA experiment uses a 6-hour spin-up initialized at 18:00 UTC every 1 day before the analysis time. In the WRF-assimilated model, the cold start assimilation process with the Rapid Update Cycle (RUC) method every 1 hour for the next 6 hours is performed as in [33,34]. This high assimilation frequency is done to take advantage of the high temporal resolution of the radiance data so that the flow tendency in the prediction model can be well captured. The WRF model was integrated to produce deterministic predictions for the next 24 hours starting at the synoptic time 00:00 UTC, June 2nd – 4th, 2019. The initial condition in the 3DVAR technique is a single data run to generate a deterministic prediction model. Whereas, in the 3DEnVar technique, the initial condition is created by 30 members using the ‘random_CV’ method that integrates Gaussian-distributed random noise into the variational analysis of the control variable space and then the ensemble mean at the last assimilation cycle is used to generate the deterministic prediction model. Model-space covariance localization in hybrid 3DEnVar is applied with a distance of 100 km in d02 and 200 km in d01 to suppress the increase of spurious correlation due to sampling error. Assimilation of AHI radians data was applied to both domains (except for the DUALRES scheme which was only applied to d02) using 3 water vapor channels (8 – 10) with a time window of ± 1 hour in each assimilation cycle. This study uses the Radiative transfer model of the Television and Infrared Observational Satellite (TIROS) Operational Vertical sounder (RTTOV) version 12 as the clear-sky radiance observation operator [35]. AHI radiances were thinned to a 9 km grid at d02 following [18,21] and 27 km at d01 to reduce potential inter-channel correlation at each radiance observation point [12].

The verification process is conducted to evaluate the WRF model's ability to simulate rainfall distribution in East Kalimantan, both before and after data assimilation, by comparing it with observational data. Two methods are used for verification: point verification, which involves comparing rainfall data at observation stations, and spatial verification by comparing to the Integrated Multi-satellitE Retrievals for GPM (IMERG) rainfall data of daily measurement

(GPM_3IMERGDF) and half-hourly measurement (GPM_3IMERGHH). Spatial verification is necessary due to the limited representation of point rainfall observation data. Point verification entails comparing measured values at 64 rain gauges with the simulated values at the nearest grid element. Spatial verification involves comparing measured values between the same grids on IMERG data with the WRF model. The IMERG data are interpolated to the same grid resolution as the WRF d02 model and then limited to the East Kalimantan region (113.8° – 119° E, 2.45° S – 2.7° N), as illustrated in Figure 1.

The final results, presented as rainfall predictions, are analyzed by comparing 3-day rainfall aggregates and hourly rainfall patterns to observe the diurnal rainfall cycle between the WRF model and observational data. The prediction skill evaluation involves analyzing the rainfall dichotomy metric, which measures the relationship between predictions (forecast) and observations (observed) in each variable category. This study calculates rainfall prediction skill based on the probability of detection (POD) metric, threat score (TS), and relative operating characteristic (ROC) curve, including the area under the ROC curve (AUC) to represent performance. Additionally, an analysis of changes in vertically integrated moisture flux convergence (VIMFC) in the 1000 – 800 hPa layer was conducted to investigate the influence of assimilation in the WRF model on the main factors of cloud and rain system formation.

3. Result and Discussion

A comparison of 3-day rainfall estimation between GPM_3IMERGDF data and the WRF model (Figure 3) reveals differences in rainfall distribution and intensity. Based on observational data, areas with rainfall intensity above 120 mm are identified in Kutai Kartanegara (west region, 115.5°E – 116°E), Balikpapan, Penajam (south region, 1°S – 2°S), Samarinda, and Mahakam River (east region, 117.5°E – 118°E). The WRF model forecasts lower rainfall over Kutai Kartanegara, with the maximum rainfall shifting to the northwest of the mountains compared to the GPM_3IMERGDF data. However, the WRF model with the DUALRES assimilation scheme provides a more accurate estimate by shifting the center of maximum rainfall to the southeast. In Balikpapan and Penajam, the WRF model demonstrates rainfall patterns that closely align with the observations but with narrower coverage. The implementation of the DUALRES scheme has been proven to enhance the accuracy of predicting rainfall distribution and intensity.

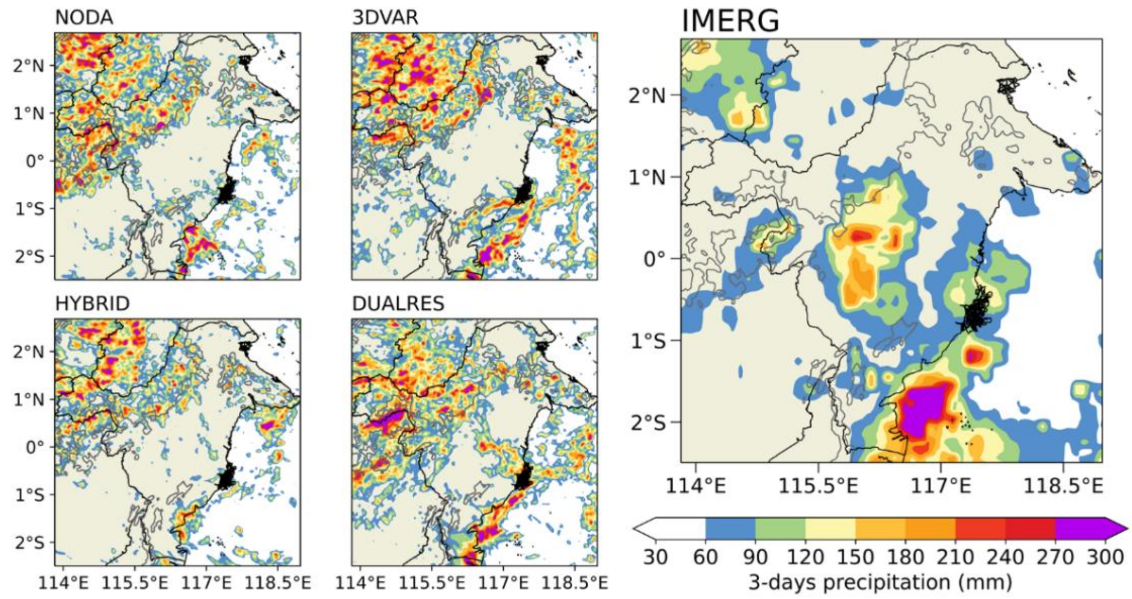

Figure 3. Aggregate rainfall for 3 days (June 2nd – 4th, 2019) obtained from GPM_3IMERGDF data and WRF model. Grey lines indicate terrain with altitude above 300 m.

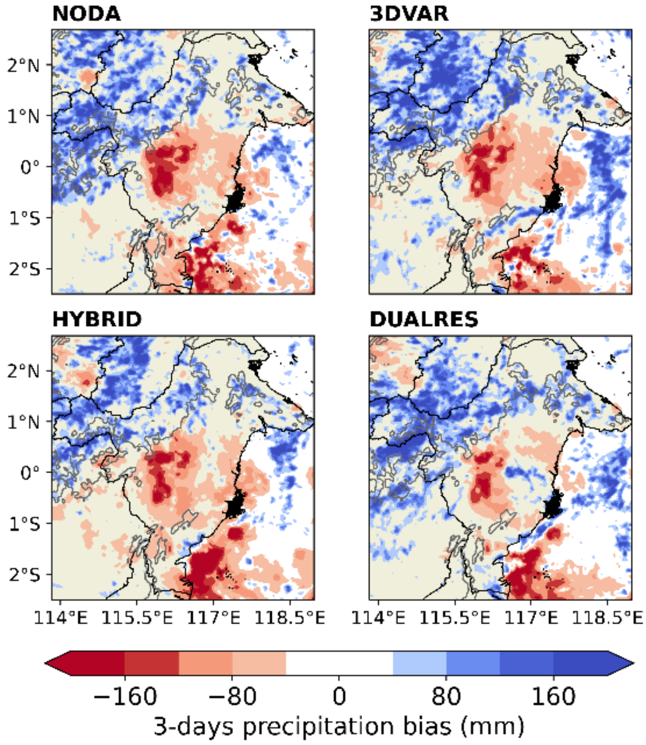

Figure 4. Bias in rainfall aggregates (WRF minus GPM_3IMERGDF model) in each scheme.

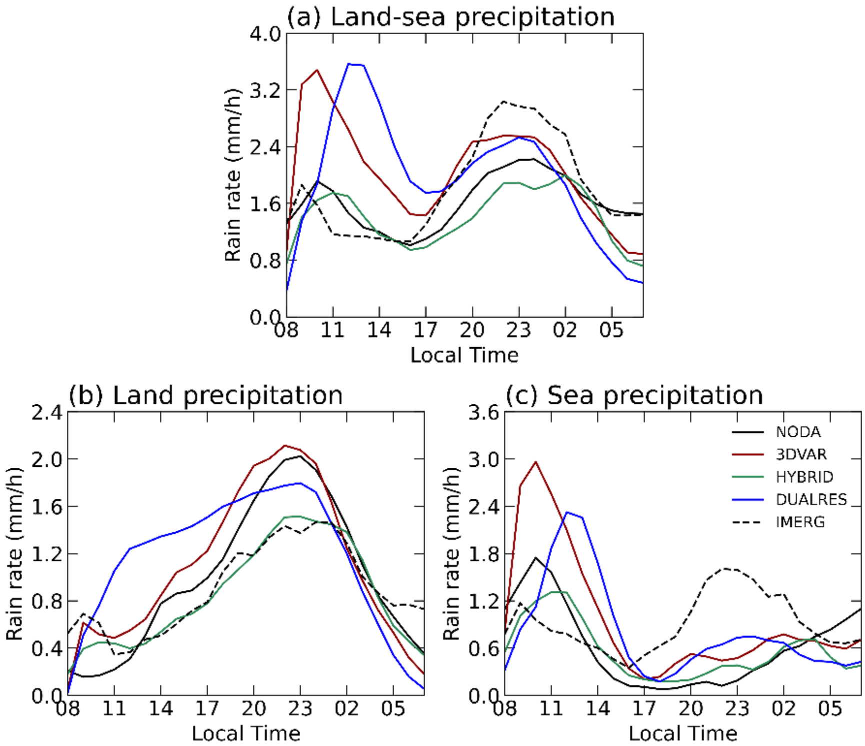

Figure 5. Hourly average rainfall pattern (June 2nd – 4th, 2019) in East Kalimantan (113.7° – 119.1° E, 2.5° S – 2.7° N) obtained from GPM_3IMERGHH data (dashed black line), NODA scheme (solid black line), 3DVAR (red line), HYBRID (green line), and DUALRES (blue line).

The comparison of rainfall bias between the WRF model and GPM_3IMERGDF data reveals specific patterns in rainfall distribution and intensity (Figure 4). The NODA scheme significantly underestimates rainfall (100-200 mm) in the center of the domain and along the Balikpapan coast, while overestimating by up to 200 mm on the western side of the hills. The 3DVAR scheme reduces the bias around the Balikpapan coast by 50% and in the center of the domain, but leads to increased underestimation in some areas. The HYBRID scheme shows a greater bias reduction than 3DVAR, with decreased bias in the west-north land area and the center of East Kalimantan, but increased underestimation in the southern water area. The DUALRES scheme demonstrates the most pronounced improvement, with decreased underestimation bias in the center of the domain and decreased overestimation bias in the west-north, resulting in more accurate rainfall estimates. Overall, the assimilation of AHI radiance reduced the rainfall bias, especially in the HYBRID and DUALRES schemes, indicating that the addition of flow-dependent covariance can enhance rainfall prediction accuracy.

Based on the diurnal rainfall pattern observed by the GPM_3IMERGHH data (Figure 5), East Kalimantan has a diurnal pattern with two rainfall peaks around 09:00 LT and 22:00 – 00:00 LT, consistent over both land and water. The NODA scheme cannot reproduce this diurnal pattern, especially in the morning, with predictions of excess rainfall over the ocean and decreased intensity over land. After the assimilation of AHI radiance data, there is an improvement although there is still a lag in the peak rainfall. The 3DVAR scheme is more accurate for land in the morning, but shows excess intensity and lag in the ocean. The HYBRID scheme improves the accuracy of the diurnal pattern, especially in the early morning, although the morning intensity is still deficient and the rainfall peak occurs later. The DUALRES scheme shows the most significant improvement with a dominant maximum intensity, despite overestimates and lags, especially over the ocean.Verification of rainfall prediction skills in East Kalimantan was carried out at the domain boundary shown by the red box in Figure 1. Figure 6 (a – c) shows the POD, TS, and ROC curves of rainfall generated by the WRF model. Based on the POD score, verification of rainfall prediction skills in East Kalimantan shows that the NODA scheme has limited performance with POD scores up to 80 mm. The 3DVAR scheme improves prediction performance up to 120 mm, with a doubling of the POD score at the 20-70 mm threshold, although lower than NODA at the 10 mm threshold. The HYBRID scheme shows consistent improvement, reaching a threshold of 140 mm with a POD score of 0.29 at 130 mm, although slightly below 3DVAR at a threshold of 20-80 mm. The DUALRES scheme showed the highest performance, improving predictions up to the 190 mm threshold with POD scores above 0.5 at the 0-160 mm threshold. As in the POD score, the NODA scheme's rainfall prediction skill using the TS metric is reliable up to an 80 mm threshold. The 3DVAR scheme increases TS up to 120 mm, and the HYBRID scheme shows consistent TS increase, reaching up to 140 mm. The DUALRES scheme performs the best, with TS increasing up to a threshold of 190 mm.

The comprehensive ROC curve analysis demonstrates the distinct rain prediction performance of each scheme. The NODA scheme exhibits the lowest performance with an AUC of 0.53, aligning closely with random prediction. Conversely, the 3DVAR scheme showcases a modest improvement with an AUC of 0.54, representing a 2% enhancement over NODA. Furthermore, the HYBRID scheme notably excels, displaying a substantial improvement with an AUC of 0.65, 23% higher than NODA, underscoring its exceptional effectiveness in predicting rainfall events. Notably, the DUALRES scheme stands out as the indisputable leader, boasting the highest true positive rate (TPR) at various false positive rate (FPR) levels and an impressive AUC of 0.66, reflecting a remarkable 25% increase and unparalleled predictive ability compared to the other schemes.

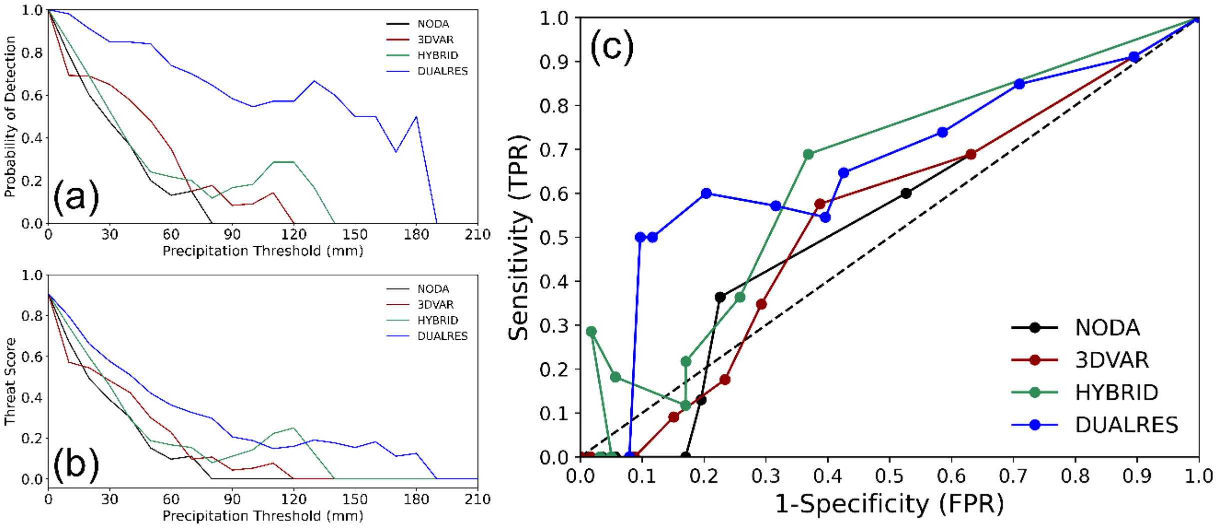

Figure 6. Rainfall scores of (a) POD, (b) TS, and (c) ROC curves for NODA (black line), 3DVAR (red line), HYBRID (green line), and DUALRES (blue line) schemes.

The analysis continued by comparing the advantages of the three AHI radiance data assimilation schemes in the convection-permitting model based on the resulting VIMFC increment. Figure 7 illustrates the difference in the percentage of VIMFC in the 1000 – 800 hPa between the NODA method and the assimilation method before, during, and after the extreme rainfall on June 2nd – 3rd, 2019 (the rainfall case on June 3rd – 4th,2019 is not shown but has the same pattern). In Figure 7, it can be seen that the increase in VIMFC occurred significantly in each assimilation scheme around the Makassar Strait with a range of increases of 50 to more than 150%. The increase in the percentage of moisture flux in this area is supported by the convergence flux pattern and the deflection of the flux direction towards the northeast, resulting in wet air accumulating around the southern waters of East Kalimantan. An increase in VIMFC also occurs from the leeward direction to the east which allows deep convection from the southeast to occur. Based on the assimilation scheme, the 3DVAR scheme provides a larger increase in moisture flux than the HYBRID and DUALRES schemes but also results in a higher decrease in moisture flux over the Sulawesi Sea by 20 – 80%.

To determine how significant the increase in VIMFC around the Makassar Strait is to changes in rainfall in East Kalimantan, a p-value significance test was conducted. Figure 8 shows the change in average rainfall (assimilation minus NODA) for each scheme overlaid by the p-value test plot of the average increase in VIMFC in the area 2.5° – 0° N and 116.5° – 119° E to the average change in rainfall in East Kalimantan on June 2nd – 4th, 2019. Black dots on the map indicate areas with a confidence level (p-value) above 99% (0.01), which means that changes in rainfall at these points are statistically significantly affected by the increase in VIMFC around the Makassar Strait.

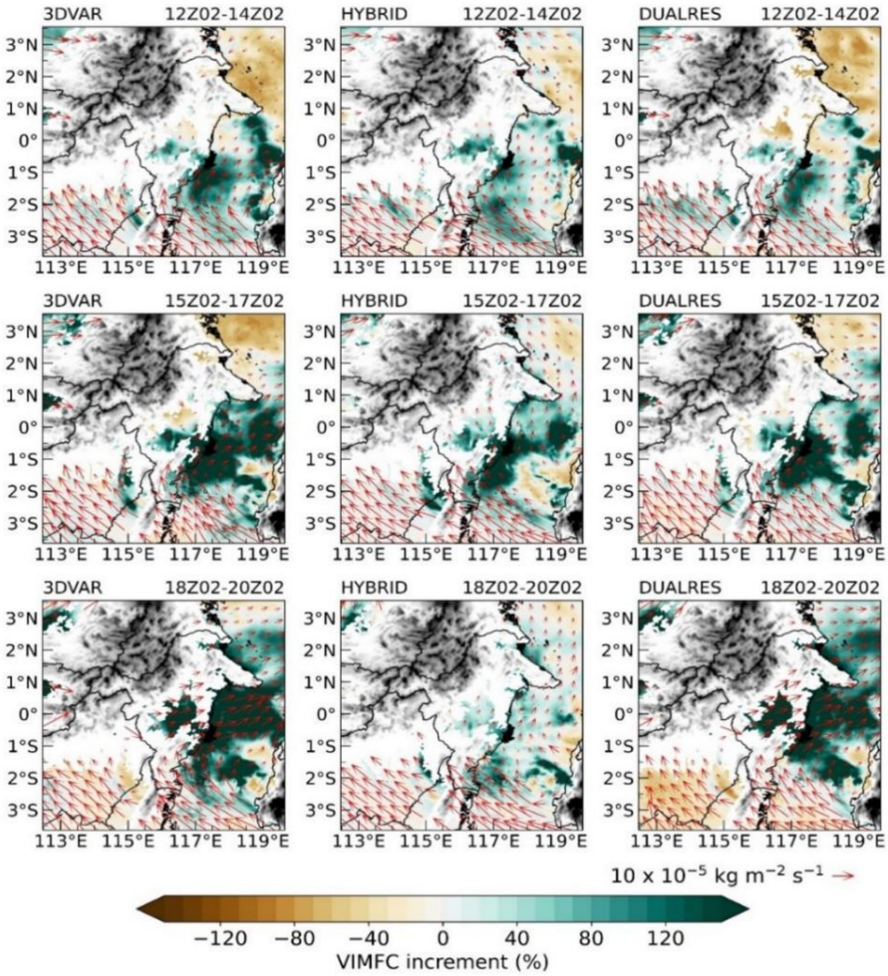

Figure 7. VIMFC increment simulated by the WRF model (assimilation minus NODA) in 3-hour averages: before, during, and after the extreme rainfall that occurred on June 2nd – 3rd, 2019. The green-brown shaded contours show the VIMFC increment in per cent, the quiver plot for the VIMFC vector in 10-5 kg m-2 s-1, and the black contours show the terrain height contours from 300 to 1500 m

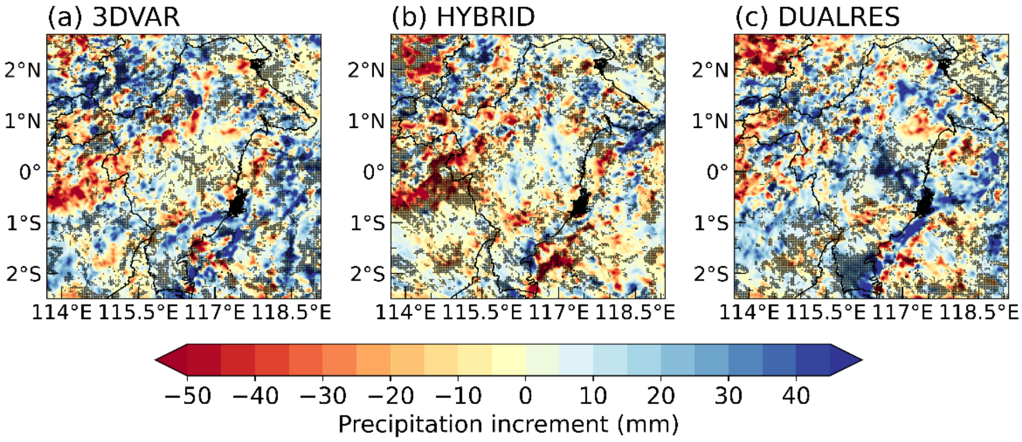

Figure 8. Average rainfall increment (assimilation minus NODA) in the (a) 3DVAR, (b) HYBRID, and (c) DUALRES schemes. Black dots represent a p-value above 99% = 0.01.

In the 3DVAR scheme (Figure 8(a)), an increase in VIMFC statistically increases rainfall by more than 15 mm in most northern regions of the domain, while in some western and central regions such as West Kutai and Kutai Kartanegara, an increase in VIMFC is indicated to decrease rainfall by up to 25 mm. This indicates that the propagation of moisture flux around the Makassar Strait in the 3DVAR scheme tends to push the increase in rainfall to the north. In the HYBRID scheme (Figure 8(b)), the increase in VIMFC statistically affects the change in rainfall intensity in most of the northwestern and some coastal and central areas of the domain. The increase in VIMFC significantly affects the increase in rainfall intensity above 25 mm that occurs around the south and northeast coast of East Kalimantan. As for the DUALRES scheme (Figure 8(c)), the increase in VIMFC around the Makassar Strait shows a more significant change in intensity widely, especially over most of the coastal and central areas of East Kalimantan. The increase in rainfall intensity in this region is higher than the other two schemes. In addition, the significance of the decrease in rainfall intensity in parts of the western and central regions affected by VIMFC changes tends to show lower results than the other two schemes. This suggests that the increase in moisture flux around the Makassar Strait in the DUALRES scheme tends to drive the increase in rainfall towards the south to the center of the domain.

4. *Conclusion*

Assimilation of Himawari-8 satellite radiance data in CPMs using 3DVAR and hybrid 3DEnVar techniques for prediction of extreme rainfall in East Kalimantan is analyzed by comparing it with models without data assimilation. In general, it was found that the assimilation of AHI data has a significant impact on improving the ability to predict and analyze extreme rainfall in East Kalimantan. Analysis of three days of rainfall in East Kalimantan showed that the WRF model with AHI radians data assimilation, especially with the DUALRES and HYBRID schemes produced more accurate simulations in predicting the distribution and intensity of rainfall than the models without assimilation (NODA) and 3DVAR. Overall, the use of assimilation schemes with the 3DEnVar method increased the accuracy of rainfall prediction and improved the diurnal rainfall pattern.

The extensive analysis of rainfall prediction skills in East Kalimantan conclusively demonstrates a significant improvement in the predictive capabilities of the WRF model when assimilating AHI radiance data, as compared to the model without assimilation (NODA). Specifically, the DUALRES scheme exhibits substantial enhancements in various evaluation metrics, including POD, TS, and ROC curves, indicating its exceptional proficiency in predicting rainfall events. The analysis firmly establishes that assimilating AHI radiance data with the HYBRID and DUALRES schemes, both applications of the 3DEnVar method, outperforms the no assimilation (NODA) and 3DVAR schemes. Additionally, the DUALRES scheme excels in improving the moisture flux analysis and enhancing evaluation metrics, underscoring its heightened sensitivity to atmospheric dynamics and its ability to produce more precise rainfall distribution and intensity while improving diurnal rainfall. As a result, the DUALRES scheme emerges as the superior choice for accurately predicting rainfall events, particularly heavy rainfall in the East Kalimantan region.

Acknowledgement

We would like to express our acknowledgement to the Indonesia Meteorological Climatological and Geophysics Agency (BMKG) and the BMKG Education and Training Centre for their financial support of the research and provision of data. We would also like to express our gratitude to the Faculty of Earth Sciences and Technology (Bandung Institute of Technology), Korea-Indonesia MTCRC (Marine Technology Cooperation Research Centre), and MAHAMERU HPC BRIN (National Research and Innovation Agency) for supporting and providing the computational services needed in this research.

References

[1] J. H. Qian, A. W. Robertson, and V. Moron, "Diurnal Cycle in Different Weather Regimes and Rainfall Variability over Borneo Associated with ENSO," *J Clim*, vol. 26, no. 5, pp. 1772–1790, Mar. 2013, doi: 10.1175/JCLI-D-12-00178.1.

[2] S. Ferrett *et al.*, "Evaluating Convection-Permitting Ensemble Forecasts of Precipitation over Southeast Asia," *Weather Forecast*, vol. 36, no. 4, pp. 1199–1217, Aug. 2021, doi: 10.1175/WAF-D-20-0216.1.

[3] S. J. Johnson *et al.*, "The resolution sensitivity of the South Asian monsoon and Indo-Pacific in a global 0.35° AGCM," *Clim Dyn*, vol. 46, no. 3–4, pp. 807–831, Feb. 2016, doi: 10.1007/S00382-015-2614-1/FIGURES/16.

[4] X. Jing *et al.*, "Convection-permitting regional climate simulations in the arabian gulf region using WRF driven by bias-corrected GCM data," *J Clim*, vol. 33, no. 18, pp. 7787–7815, Sep. 2020, doi: 10.1175/JCLI-D-20-0155.1.

[5] N. J. Weber and C. F. Mass, "Subseasonal Weather Prediction in a Global Convection-Permitting Model," *Bull Am Meteorol Soc*, vol. 100, no. 6, pp. 1079–1089, Jun. 2019, doi: 10.1175/BAMS-D-18-0210.1.

[6] C. L. Vincent and T. P. Lane, "A 10-Year Austral Summer Climatology of Observed and Modeled Intraseasonal, Mesoscale, and Diurnal Variations over the Maritime Continent," *J Clim*, vol. 30, no. 10, pp. 3807–3828, May 2017, doi: 10.1175/JCLI-D-16-0688.1.

[7] L. Zhu, Z. Meng, Y. Weng, and F. Zhang, "Assimilation of All-sky Geostationary Satellite Infrared Radiances for Convection-Permitting Initialization and Prediction of Hurricane Joaquin (2015)," *Adv Atmos Sci*, 2022, doi: 10.1007/s00376-022-2015-4.

[8] Z. Qin, X. Zou, and F. Weng, "Impacts of assimilating all or GOES-like AHI infrared channels radiances on QPFs over Eastern China," *Tellus, Series A: Dynamic Meteorology and Oceanography*, vol. 69, no. 1, Jul. 2017, doi: 10.1080/16000870.2017.1345265.

[9] K. Bessho *et al.*, "An Introduction to Himawari-8/9— Japan's New-Generation Geostationary Meteorological Satellites," *Journal of the Meteorological Society of Japan. Ser. II*, vol. 94, no. 2, pp. 151–183, 2016, doi: 10.2151/JMSJ.2016-009.

[10] K. Okamoto, Y. Sawada, and M. Kunii, "Comparison of assimilating all-sky and clear-sky infrared radiances from Himawari-8 in a mesoscale system," *Quarterly Journal of the Royal Meteorological Society*, vol. 145, no. 719, pp. 745–766, Jan. 2019, doi: 10.1002/QJ.3463.

[11] Y. Sawada, K. Okamoto, M. Kunii, and T. Miyoshi, "Assimilating Every-10-minute Himawari-8 Infrared Radiances to Improve Convective Predictability," *Journal of Geophysical Research: Atmospheres*, vol. 124, no. 5, pp. 2546–2561, Mar. 2019, doi: 10.1029/2018JD029643.

[12] Z. Ma, E. S. Maddy, B. Zhang, T. Zhu, and S. A. Boukabara, "Impact Assessment of Himawari-8 AHI Data Assimilation in NCEP GDAS/GFS with GSI," *J Atmos Ocean Technol*, vol. 34, no. 4, pp. 797–815, Apr. 2017, doi: 10.1175/JTECH-D-16-0136.1.

[13] B. S. Nugroho, "PENGARUH ASIMILASI DATA SATELIT HIMAWARI-8 PADA PEMODELAN CUACA WRF-ARW UNTUK PREDIKSI SIKLON TROPIS," *ejurnal.bppt.go.id*, vol. 23, no. 1, pp. 11–25, 2022, Accessed: Nov. 06, 2022. [Online]. Available: https://ejurnal.bppt.go.id/index.php/JSTMC/article/view/5236

[14] F. Shen, A. Shu, H. Li, D. Xu, and J. Min, "Assimilation of Himawari-8 imager radiance data with the WRF-3DVAR system for the prediction of Typhoon Soudelor," *Natural Hazards and Earth System Sciences*, vol. 21, no. 5, pp. 1569–1582, 2021, doi: 10.5194/nhess-21-1569-2021.

[15] M. Minamide and F. Zhang, "Assimilation of All-Sky Infrared Radiances from Himawari-8 and Impacts of Moisture and Hydrometer Initialization on Convection-Permitting Tropical Cyclone Prediction," *Mon Weather Rev*, vol. 146, no. 10, pp. 3241–3258, Oct. 2018, doi: 10.1175/MWR-D-17-0367.1.

[16] T. Honda *et al.*, "Assimilating All-Sky Himawari-8 Satellite Infrared Radiances: A Case of Typhoon Soudelor (2015)," *Mon Weather Rev*, vol. 146, no. 1, pp. 213–229, Jan. 2018, doi: 10.1175/MWR-D-16-0357.1.

[17] J. Wang, L. Zhang, J. Guan, X. Wang, M. Zhang, and Y. Wang, "Potential Impacts of Assimilating Every-10-Minute Himawari-8 Satellite Radiance with the POD-4DEnVar Method," *Remote Sensing 2021, Vol. 13, Page 3765*, vol. 13, no. 18, p. 3765, Sep. 2021, doi: 10.3390/RS13183765.

[18] D. Xu, Z. Liu, S. Fan, M. Chen, and F. Shen, "Assimilating All-sky Infrared Radiances from Himawari-8 Using the 3DVar Method for the Prediction of a Severe Storm over North China," *Adv Atmos Sci*, vol. 38, no. 4, pp. 661–676, Apr. 2021, doi: 10.1007/s00376-020-0219-z.

[19] Y. Wu, Z. Liu, and D. Li, "Improving forecasts of a record-breaking rainstorm in Guangzhou by assimilating every 10-min AHI radiances with WRF 4DVAR," *Atmos Res*, vol. 239, p. 104912, Jul. 2020, doi: 10.1016/J.ATMOSRES.2020.104912.

[20] T. Honda, S. Kotsuki, G. Y. Lien, Y. Maejima, K. Okamoto, and T. Miyoshi, "Assimilation of Himawari-8 All-Sky Radiances Every 10 Minutes: Impact on Precipitation and Flood Risk Prediction," *Journal of Geophysical Research: Atmospheres*, vol. 123, no. 2, pp. 965–976, Jan. 2018, doi: 10.1002/2017JD027096.

[21] Y. Wang *et al.*, "Added Value of Assimilating Himawari-8 AHI Water Vapor Radiances on Analyses and Forecasts for '7.19' Severe Storm Over North China," *Journal of Geophysical Research: Atmospheres*, vol. 123, no. 7, pp. 3374–3394, Apr. 2018, doi: 10.1002/2017JD027697.

[22] J. S. Whitaker and T. M. Hamill, "Ensemble data assimilation without perturbed observations," *Mon Weather Rev*, vol. 130, no. 7, pp. 1913–1924, 2002, doi: 10.1175/1520-0493(2002)130<1913:EDAWPO>2.0.CO;2.

[23] T. M. Hamill and C. Snyder, "A hybrid ensemble Kalman filter-3D variational analysis scheme," *Mon Weather Rev*, vol. 128, no. 8 II, pp. 2905–2919, 2000, doi: 10.1175/1520-0493(2000)128<2905:ahekfv>2.0.co;2.

[24] X. Wang, "Application of the WRF Hybrid ETKF–3DVAR Data Assimilation System for Hurricane Track Forecasts," *Weather Forecast*, vol. 26, no. 6, pp. 868–884, 2011, doi: https://doi.org/10.1175/WAF-D-10-05058.1.

[25] W. C. Skamarock *et al.*, "A Description of the Advanced Research WRF Model Version 4.3," 2021, doi: 10.5065/1DFH-6P97.

[26] S. Hong and J. Lim, "The WRF Single-Moment 6-Class Microphysics Scheme (WSM6)," *Asia Pac J Atmos Sci*, 2006.

[27] S. Y. Hong, Y. Noh, and J. Dudhia, "A New Vertical Diffusion Package with an Explicit Treatment of Entrainment Processes," *Mon Weather Rev*, vol. 134, no. 9, pp. 2318–2341, Sep. 2006, doi: 10.1175/MWR3199.1.

[28] E. J. Mlawer, S. J. Taubman, P. D. Brown, M. J. Iacono, and S. A. Clough, "Radiative transfer for inhomogeneous atmospheres: RRTM, a validated correlated-k model for the longwave," *Journal of Geophysical Research: Atmospheres*, vol. 102, no. D14, pp. 16663–16682, Jul. 1997, doi: 10.1029/97JD00237.

[29] J. Dudhia, “Numerical Study of Convection Observed during the Winter Monsoon Experiment Using a Mesoscale Two-Dimensional Model,” *Journal of Atmospheric Sciences*, vol. 46, no. 20, pp. 3077–3107, 1989, doi: https://doi.org/10.1175/1520-0469(1989)046<3077:NSOCOD>2.0.CO;2.

[30] N. M. Tewari, M. Tewari, F. Chen, and ..., “Implementation and verification of the unified NOAH land surface model in the WRF model,” *20th Conference on Weather Analysis and Forecasting/16th Conference on Numerical Weather Prediction*, 2004, [Online]. Available: https://ams.confex.com/ams/84Annual/techprogram/paper_69061.htm

[31] J. S. Kain, “The Kain-Fritsch Convective Parameterization: An Update,” *Journal of applied meteorology*, vol. 43, pp. 170–181, 2004.

[32] H. Wang *et al.*, “Inhomogeneous background error modeling for WRF-var using the NMC method,” *J Appl Meteorol Climatol*, vol. 53, no. 10, pp. 2287–2309, 2014, doi: 10.1175/JAMC-D-13-0281.1.

[33] Y. Wang, Y. Chen, and J. Min, “Improving the prediction of heavy rainfall with rapid-update dual-resolution hybrid En3DVar assimilation of all-sky AHI infrared water vapor radiances,” *Atmos Res*, vol. 279, 2022, doi: 10.1016/J.ATMOSRES.2022.106352.

[34] X. Li, X. Zou, X. Zhuge, M. Zeng, N. Wang, and F. Tang, “Improved Himawari-8/AHI Radiance Data Assimilation With a Double Cloud Detection Scheme,” *Journal of Geophysical Research: Atmospheres*, vol. 125, no. 13, 2020, doi: 10.1029/2020JD032631.

[35] R. Saunders *et al.*, “An update on the RTTOV fast radiative transfer model (currently at version 12),” *Geosci Model Dev*, vol. 11, no. 7, pp. 2717–2737, Jul. 2018, doi: 10.5194/GMD-11-2717-2018.

[36] G. J. Zhang and X. Song, “Parameterization of Microphysical Processes in Convective Clouds in Global Climate Models,” *Meteorological Monographs*, vol. 56, no. 24, pp. 1–18, 2016.

[37] Y. Kogan, “A Cumulus Cloud Microphysics Parameterization for Cloud- Resolving Models,” *J Atmos Sci*, vol. 70, no. 14, pp. 23–36.